

High-performance midwavelength infrared detectors based on InAsSb nBn design

Xuan Zhang(张璇), Qing-Xuan Jia(贾庆轩), Ju Sun(孙矩), Dong-Wei Jiang(蒋洞微), Guo-Wei Wang(王国伟), Ying-Qiang Xu(徐应强), Zhi-Chuan Niu(牛智川)

Citation: Chin. Phys. B . 2020, 29(6): 068501 . **doi:** 10.1088/1674-1056/ab8377
Journal homepage: http://cpb.iphy.ac.cn; http://iopscience.iop.org/cpb

What follows is a list of articles you may be interested in

Ultraviolet irradiation dosimeter based on persistent photoconductivity effect of ZnO

Chao-Jun Wang(王朝骏), Xun Yang(杨珣), Jin-Hao Zang(臧金浩), Yan-Cheng Chen(陈彦成), Chao-Nan Lin(林超男), Zhong-Xia Liu(刘忠侠), Chong-Xin Shan(单崇新)

Chin. Phys. B . 2020, 29(5): 058504 . **doi:** 10.1088/1674-1056/ab8891

A method to extend wavelength into middle-wavelength infrared based on InAsSb/(Al)GaSb interband transition quantum well infrared photodetector

Xuan-Zhang Li(李炫璋), Ling Sun(孙令), Jin-Lei Lu(鲁金蕾), Jie Liu(刘洁), Chen Yue(岳琛), Li-Li Xie(谢莉莉), Wen-Xin Wang(王文新), Hong Chen(陈弘), Hai-Qiang Jia(贾海强), Lu Wang(王禄)

Chin. Phys. B . 2020, 29(3): 038504 . **doi:** 10.1088/1674-1056/ab6969

High quantum efficiency long-/long-wave dual-color type-Ⅱ InAs/GaSb infrared detector

Zhi Jiang(蒋志), Yao-Yao Sun(孙姚耀), Chun-Yan Guo(郭春妍), Yue-Xi Lv(吕粤希), Hong-Yue Hao(郝宏玥), Dong-Wei Jiang(蒋洞微), Guo-Wei Wang(王国伟), Ying-Qiang Xu(徐应强), Zhi-Chuan Niu(牛智川)

Chin. Phys. B . 2019, 28(3): 038504 . **doi:** 10.1088/1674-1056/28/3/038504

Development of long-wavelength infrared detector and its space-based application requirements

Junku Liu(刘军库), Lin Xiao(肖林), Yang Liu(刘阳), Longfei Cao(曹龙飞), Zhengkun Shen(申正坤)

Chin. Phys. B . 2019, 28(2): 028504 . **doi:** 10.1088/1674-1056/28/2/028504

High material quality growth of AlInAsSb thin films on GaSb substrate by molecular beam epitaxy

Fa-Ran Chang(常发冉), Rui-Ting Hao(郝瑞亭), Tong-Tong Qi(齐通通), Qi-Chen Zhao(赵其琛), Xin-Xing Liu(刘欣星), Yong Li(李勇), Kang Gu(顾康), Jie Guo(郭杰), Guo-Wei Wang(王国伟), Ying-Qiang Xu(徐应强), Zhi-Chuan Niu(牛智川)

Chin. Phys. B . 2019, 28(2): 028503 . **doi:** 10.1088/1674-1056/28/2/028503

High-performance midwavelength infrared detectors based on InAsSb nBn design*

Xuan Zhang(张璇)[1,2], Qing-Xuan Jia(贾庆轩)[1,2], Ju Sun(孙矩)[1,2], Dong-Wei Jiang(蒋洞微)[1,2,3], Guo-Wei Wang(王国伟)[1,2,3,†], Ying-Qiang Xu(徐应强)[1,2,3], and Zhi-Chuan Niu(牛智川)[1,2,3,4,‡]

[1] *State Key Laboratory for Superlattices and Microstructures, Institute of Semiconductors, Chinese Academy of Sciences, Beijing* 100083, *China*
[2] *College of Materials Science and Opto-Electronic Technology, University of Chinese Academy of Sciences, Beijing* 101408, *China*
[3] *Center of Materials Science and Optoelectronics Engineering, College of Materials Science and Opto-Electronic Technology, University of Chinese Academy of Sciences, Beijing* 100049, *China*
[4] *Beijing Academy of Quantum Information Sciences, Beijing* 100193, *China*

(Received 15 February 2020; revised manuscript received 15 March 2020; accepted manuscript online 26 March 2020)

we report nBn photodetectors based on $InAs_{0.91}Sb_{0.09}$ with a 100% cut-off wavelength of 4.75 μm at 300 K. The band of an nBn detector is similar to that of a standard pin detector, but there is special wide bandgap $AlAs_{0.08}Sb_{0.92}$ barrier layer in the nBn detector, in which the depletion region of nBn detector exists. The nBn design has many advantages, such as low dark current and high quantum efficiency, because the nBn design can suppress the generation–recombination (GR) current that is the main composition of standard pin detector dark current. The constant slope of the Arrhenius plot of J_0–$1/T$ indicates the absence of the generation–recombination dark current. We fabricate an nBn detector with a quantum efficiency (QE) maximum of ∼60% under −0.2-V bias voltage. The InAsSb nBn detectors may be a competitive candidate for midwavelength infrared detector.

Keywords: infrared detector, InAsSb, nBn

PACS: 85.60.Gz, 72.20.Jv **DOI:** 10.1088/1674-1056/ab8377

1. Introduction

Due to long Auger lifetime and other advantages, InAs/Gasb superlattice material system has become a candidate material for replacing HgCdTe (MCT).[1,2] However, the detector fabricated by an InAs/Gasb superlattice material system has a relatively high dark-current. The high generation–recombination (GR) dark current is caused by a low Shockley–Rad–Hall (SRH) lifetime, which results from the original defects of the GaSb layer.[3–5]

As a typical III–V ternary compound semiconductor material, the structure of InAsSb is stable. There is a stable chemical bond between indium (In) and arsenic (As) or antimony (Sb). Compared with MCT, the InAsSb has a high carrier mobility and relatively small dielectric constant and self-diffusion coefficient at room temperature. Therefore, the InAsSb has become an important candidate for fabricating midwavelength infrared (MWIR) detectors and optical gas sensors.

As figure 1(a) shows, the diffusion current at low temperature is several orders of magnitude lower than the generation–recombination current, while at high temperature it is several orders greater.[6] Define T_0 as the "cross-over" temperature at which the diffusion and generation–recombination currents are equal then we will be able to use a function of the bandgap of the InAsSb absorbing layer to estimate the values of T_0.[7] For an nBn detector, there exists a depletion region in the wide bandgap barrier, so the generation–recombination dark current is suppressed.[7–9] Figure 1(a) shows a typical Arrhenius plot of the dark current in a pin detector. The slope of the lower line is about half that of the upper line. When multiplied by Boltzman's constant, these two slopes essentially correspond to the activation energy for generation–recombination and diffusion limited behavior, respectively. The dotted line is an extension of the diffusion limited behavior to the case of low temperature. At temperatures below T_0, the nBn detector presents the following two important advantages.

(i) The dark current density is lower than that of pin detector working at the same temperature.

(ii) The nBn detector can operate at a higher temperature than the pin detector under the same dark current.

They are indicated by solid and dotted arrows in Fig. 1, respectively. Figure 1(b) shows the band profile of an nBn detector with an n-type barrier layer. Further discussion of the principles of nBn detector can be found in other papers.[10–12]

*Project supported by the National Key Technologies Research and Development Program of China (Grant No. 2018YFA0209104) and the Major Program of the National Natural Science Foundation of China (Grant No. 61790581).

†Corresponding author. E-mail: wangguowei@semi.ac.cn
‡Corresponding author. E-mail: zcniu@semi.ac.cn

© 2020 Chinese Physical Society and IOP Publishing Ltd

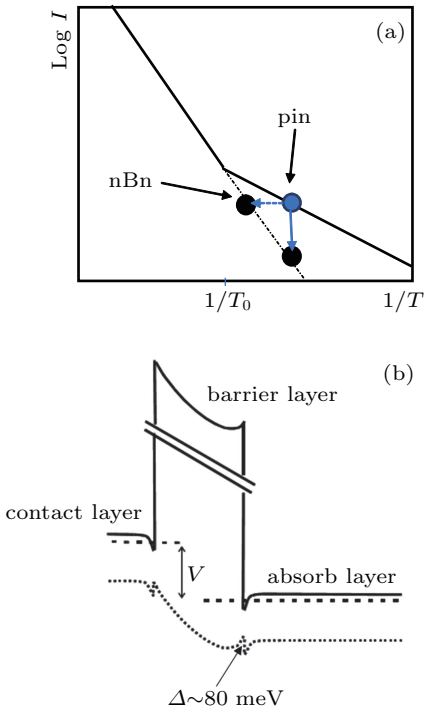


Fig. 1. (a) Arrhenius plot of dark current in pin detector (solid line) and nBn detector (dotted line).[6] (b) Band profile of nBn detector with n-type barrier layer, at operating bias.

2. Experimental methods

In this work, our samples were grown with Veeco Gen20 molecular beam epitaxy (MBE) system with group III cells and group V valved cracker cells in this experiment. The rate ratio of As to Sb was kept at 0.91 : 0.09 throughout the growth progress, and the growth rate of In was 0.5 ML/s, that was measured with reflection high energy electron diffraction (RHEED) prior to growth. We used flux monitor and GaSb (001) surface reconstruction to calibrate the V/III ratio and substrate temperature. For more imformation about growth progress and techniques readers may refer to other relevent literature.

As figure 2 shows, the nBn detcetor consists of a 0.5–μm-thick n-GaSb buffer layer, 1-μm-thick n^+-$InAs_{0.91}Sb_{0.09}$ (5×10^{17} cm^{-3}) bottom contact layer, 2.5-μm-thick n-$InAs_{0.91}Sb_{0.09}$ (1×10^{16} cm^{-3}) absorption layer, 0.2-μm-thick n-doped $AlAs_{0.08}Sb_{0.92}$ barrier layer, and 0.25-μm-thick n^+-InAsSb (5×10^{17} cm^{-3}) top contact layer. The other sample, InAsSb pin detector, was grown for comparison. The pin structure was grown with GaSb buffer layer, 0.5-μm-thick p^+-InAsSb (1×10^{18} cm^{-3}), 2-μm-thick undoped InAsSb active layer, and 0.5-μm-thick n^+-InAsSb (1.2×10^{18} cm^{-3}) layer which is a top contact layer. The doping in nBn sample and that in pin sample were achieved by silicon (Si) and beryllium (Be) during growth, respectively. We used high resolution x-ray diffraction (HRXRD) and atomic force microscopy (AFM) to characterize the layer structure and material quality.

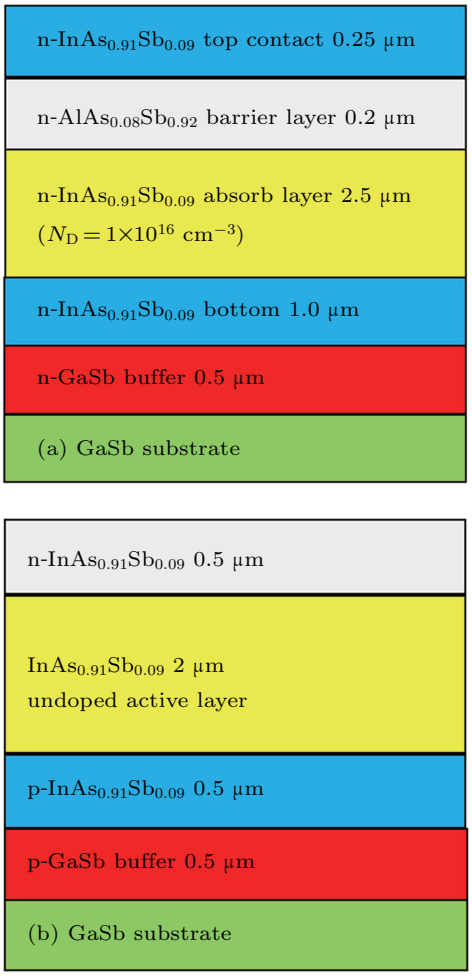


Fig. 2. Epitaxial structure of (a) nBn detector and (b) pin.

Figure 3 shows the HRXRD and AFM image of an nBn sample. The sample exhibits clear atomic step with a root mean square (RMS) surface roughness of 1.82 Å over an area of 10 μm×10 μm. The HRXRD rocking curve shows that the splitting between InAsSb layer and GaSb layer is 64 arcsec and the full width at half maximum (FWHM) of InAsSb layers is ∼ 50 arcsec in many experiments. As shown by the surface morphology, AFM, and HRXRD data, the growth conditions of InAsSb layers are appropriate, which is the reason why we can achieve a thick enough InAsSb layer without dislocations or other growth defects introduced by lattice mismatch. The AlAsSb barrier layer can also be optimized, as InAsSb layer is optimized. The pin sample is also characterized by the AFM and HRXRD. The pin sample exhibits a clear atomic step of 1.99-Å RMS surface roughness over an area of 10 μm ×10 μm and a 40-arcsec splitting between InAsSb layers and GaSb substrate, but we do not show these data here. Figure 4 shows the splitting mapping over a whole 3″ wafer. Each colour in Fig. 4 corresponds to a splitting value and the splitting varies radially between the center and edge of the wafer, with a total splitting value of about 60 arcsec. We believe that these HRXRD results demonstrate a high uniformity for MBE growth. After characterization, we use a standard de-

tector fabrication process, which includes 4 times lithography process and etching process by inductively coupled plasma (ICP).

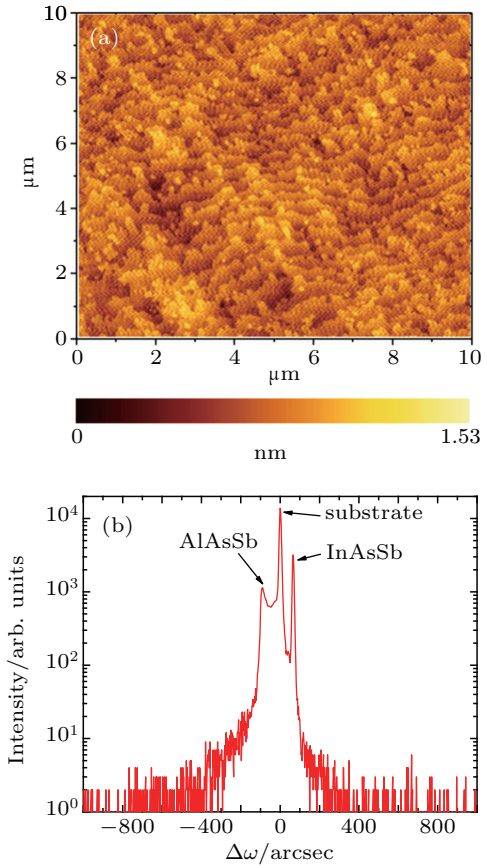


Fig. 3. (a) AFM of an area of 10 μm×10 μm for nBn sample; (b) HRXRD rocking curve for nBn sample.

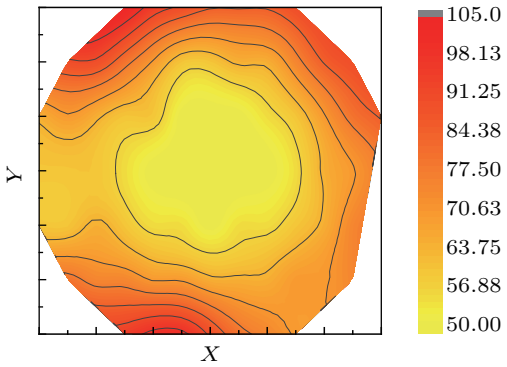


Fig. 4. HRXRD mapping of nBn sample on 3″ wafer.

3. Experimental results and discussion

Figure 5 shows dark current density characteristics of nBn detector and pin detector at temperatures ranging from 150 K to 300 K. The dark current density of nBn detector is 8.95×10^{-6} A/cm^2 and 1.7 A/cm^2 under −0.2-V bias voltage at 150 K and 300 K, respectively. The constant slope in the figure indicates the absence of GR dark current. There is only slightly difference from the theory ($T^s\exp(-E/kT)$ (E is the activation energy), which results from other reason, such as surface leakage current.

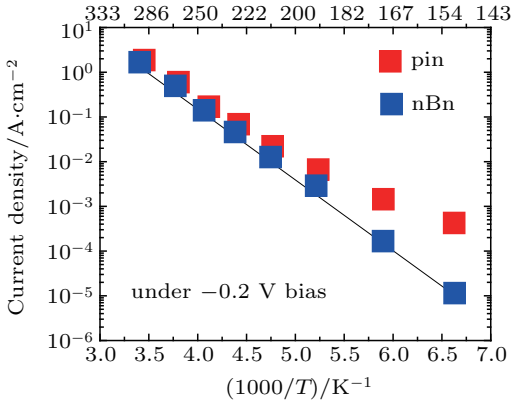


Fig. 5. Arrhenius plot of dark current in pin detector (red dot) and nBn detector (blue dot) under −0.2 V at 300 K.

Figure 6 shows the curves of quantum efficiency (QE) *versus* λ of pin and nBn detectors at room temperature. We use a Fourier transform infrared spectrometer and a blackbody to measure the spectral response, and the quantum efficiency, respectively. As figure 6 shows, pin detector has a 100% cut-off wavelength of 4.8 μm and 50% cut-off wavelength of 4.4 μm. The QE of pin detector achieves its maximum of 41.4% at 4.1 μm. As figure 6 shows, the nBn detector has a 100% cut-off wavelength of 4.75 μm at 300 K. The QE of nBn detector reaches its peak of 30.1% at 4.05 μm under 0-V bias; when we apply a −0.2-V bias voltage to nBn detector, the QE maximum goes up to 63.4%. As bias increases, the QE values of nBn detectors increase.[13] QE maximum value under −0.2 V reaches > 90% of that under −0.6 V in our nBn detector. The QE values of these detectors-based InAsSb are all higher than those of InAs/GaSb type-II supperlattice pin detectors. There is a little difference in cut-off wavelength between nBn detector and pin detector. It is believed that the cut-off wavelength difference results from little difference in ratio among V group elements caused by MBE growth and difference in doping.

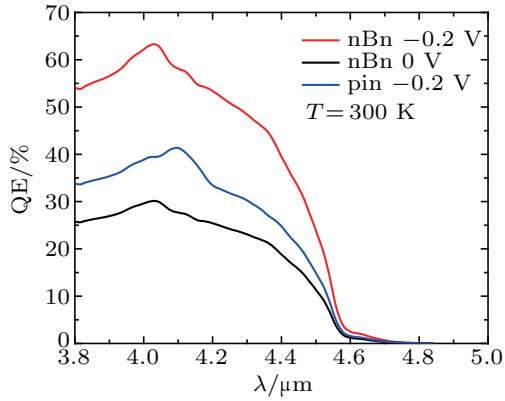


Fig. 6. Curves of QE *versus* λ of pin and nBn detectors under different bias voltages at 300 K.

According to the measured spectral data, such as J and RA, we can calculate specific detectivity (D^*) values of pin

and nBn detectors from the following equation:

$$D^* = \frac{\lambda}{hc} q\eta \left(2qJ + \frac{4KT}{RA}\right)^{-1/2}, \quad (1)$$

where K is the Boltzmann constant, and h is the Planck constant. The two items in the brackets are related to shot noise and Johnson noise, respectively. Figure 7 shows that the pin detector exhibits a peak specific detectivity of 1.4×10^9 cm·Hz$^{1/2}$/W. The nBn detector exhibits a peak specific detectivity of 8.5×10^8 cm·Hz$^{1/2}$/W and 2.3×10^9 cm·Hz$^{1/2}$/W under 0-V and −0.2-V bias voltages at 300 K, respectively. The combined contributions of enhanced QE and reduced noise result in the greater enhancement of D^* for nBn detector under −0.2-V bias voltage.

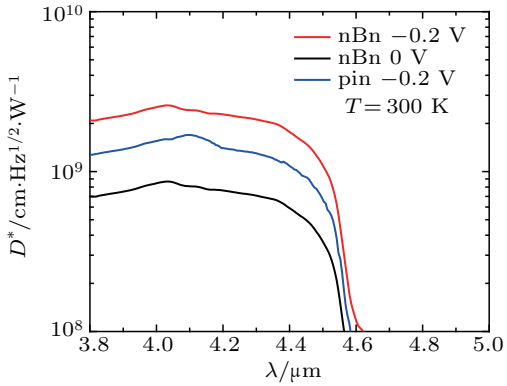


Fig. 7. Curves of D^* *versus* λ of pin and nBn detectors under different bias voltages at 300 K.

4. Conclusions

In summary, Arrhenius plot of J_{dark}–$1/T$ shows that GR current is completely suppressed in InAsSb nBn detectors in a temperature range from 150 K to 300 K, which limits the performance of pin detector. The nBn detector achieves a QE of ∼ 63.4% under −0.2 V at 300 K, which is higher than the QE values of type-II InAs/Gasb superlattice MWIR detectors. There is still room for improvement, but these good experimental data show that the InAsSb nBn detector may be a candidate for MWIR detector.

References

[1] Youngdale E R, Meyer J R, Hoffman C A, Bartoli F J, Grein C H, Young P M, Ehrenreich H, Miles R H and Chow D H 1994 *Appl. Phys. Lett.* **64** 3160

[2] Yen L T, Yoshinan K and Nobuya M 2019 *Jpn. J. Appl. Phys.* **58** 081003

[3] Donetsky D, Svensson S P, Vorobjev L E and Belenky G 2009 *Appl. Phys. Lett.* **95** 212104

[4] Svensson S P, Donetsky D, Wang D, Hier H, Crowne F J and Belenky G 2011 *J. Cryst. Growth* **334** 103

[5] Grein C H, Garland J and Flatte M E 2009 *J. Electron. Mater.* **38** 1800

[6] Philip K, Olga K, Steve G, Noam S, Inna L, Daniel A, Michael Y, Alex G, Tal F, Eyal B, Osnat M, Itay S, Eliezer W 2011 *Opt. Eng.* **50** 061002

[7] Haddadi A, Chevallier R, Dehzangi A and Razeghi M 2017 *Appl. Phys. Lett.* **110** 101104

[8] Maimon S and Wicks G W 2006 *Appl. Phys. Lett.* **89** 151109

[9] Soibel A, Ting D Z, Hill C J, Fisher A M, Hoglund L, Keo S A and Gunapala S D 2016 *Appl. Phys. Lett.* **109** 103505

[10] Pepper B, Soibel A, Ting D, Hill C, Khoshakhlagh A, Fisher A, Keo S and Gunapala S 2019 *Infrared Phys. Technol.* **99** 64

[11] Ting D Z, Soibel A, Khoshakhlagh A, Keo S A, Rafol S B, Fisher A M, Pepper B J, Luong E M, Hill C J and Gunapala S D 2019 *Infrared Phys. Technol.* **97** 210

[12] Wang P, Xia H, Li Q, Wang F, Zhang L, Li T, Martyniuk P, Rogalski A and Hu W 2019 *Small* **15** 1904396

[13] Johnson J L, Samoska L A, Gossard A C, Merz J L, Jack M D, Chapman G R, Baumgratz B A, Kosai K and Johnson S M 1996 *J. Appl. Phys.* **80** 1116